# Crystal, Molecular and Electronic Structure of *N*,*N*′-Diphenyl-*N*,*N*′-bis(2,4-dimethylphenyl)-(1,1′-biphenyl)-4,4′-diamine and the Corresponding Radical Cation

**Paul J. Low,*[a] Michael A. J. Paterson,[a] Horst Puschmann,[a] Andrés E. Goeta,[a] Judith A. K. Howard,[a] Christoph Lambert,[b] Julian C. Cherryman,[c] Daniel R. Tackley,[c] Stephen Leeming,[c] and Bev Brown[c]**

**Abstract:** Oxidation of *N*,*N*′-diphenyl-*N*,*N*′-bis(3-methylphenyl)-(1,1′-biphenyl)-4,4′-diamine (TPD, **1a**) and *N*,*N*′-diphenyl-*N*,*N*′-bis(2,4-dimethylphenyl)-(1,1′-biphenyl)-4,4′-diamine (**1b**) with $SbCl_5$ affords the corresponding radical cations quantitatively. The crystal and molecular structure of **1b** and [**1b**]$SbCl_6$, the first tetraphenyl benzidene derivatives to be characterised crystallographically in both the neutral and radical cation states, reveal molecular parameters in agreement with the predictions made on the basis of DFT studies. Analysis of the NIR transition in the radical cations $[\mathbf{1}]^{+\cdot}$ allows an estimate of the electronic coupling parameter $V$ ($\mathbf{1a}^{+\cdot}$ 3200 $cm^{-1}$; $\mathbf{1b}^{+\cdot}$ 3300 $cm^{-1}$), the reorganisation energy $\lambda$($\mathbf{1a}^{+\cdot}$ 7500 $cm^{-1}$; $\mathbf{1b}^{+\cdot}$ 7800 $cm^{-1}$), and the linear coupling constant $l$ ($\mathbf{1a}^{+\cdot}$ 3100 $cm^{-1}$; $\mathbf{1b}^{+\cdot}$ 2700 $cm^{-1}$) of the symmetric mode.

**Keywords:** amines · biaryls · charge carrier injection · electron transfer · radical ions

## Introduction

At the present time there is intense interest in the structure and electronic properties of *N*,*N*,*N*′,*N*′-tetraaryl-(1,1′-biphenyl)-4,4′-diamines, as these materials are used as the vital hole injecting and transporting layers in a wide range of electro-optic devices.[1] Establishing relationships between the molecular structure of these compounds and physical characteristics such as oxidation (or ionisation) potential,[2] packing arrangement in the solid state,[3] reorganisation energy upon charge transfer,[4] and environmental stability[5] is of considerable interest, as each of these properties will influence the hole transport performance of the compound in a device.

The hole transport properties of a compound can be represented in terms of a hopping model, which can be approximated in terms of an electron transfer event between a neighbouring neutral molecule, N, and its corresponding radical cation, $N^{+\cdot}$ [Eq. (1)].[6]

$$N_A + [N_B]^{+\cdot} \rightarrow [N_A]^{+\cdot} + N_B \quad (1)$$

Since the components on the left and right side of the equation are the same, the net free energy for the reaction $\Delta G^0$ is zero and the activation barrier to *inter*molecular charge migration, $\Delta G^{\neq}$, should be $\lambda/4$, where $\lambda$ is the re-organisation energy associated with geometric rearrangement from both the neutral to charged state and from the charged state to the neutral, and will include a contribution from the supporting medium. It follows that minimising $\lambda$ is one factor that may lead to improved hole mobility. Therefore, a detailed understanding of the molecular parameters associated with both the neutral and radical forms of a charge transport material would be of great interest.

Malagoli and Brédas have recently reported a computational study of the reorganisation energy associated with the oxidation of *N*,*N*′-diphenyl-*N*,*N*′-bis(3-methylphenyl)-(1,1′-

[a] Dr. P. J. Low, M. A. J. Paterson, Dr. H. Puschmann, Dr. A. E. Goeta, Prof. J. A. K. Howard
Department of Chemistry, University of Durham
South Road, Durham, DH1 3LE (UK)
Fax: (+44) 191-374-2101
E-mail: p.j.low@durham.ac.uk

[b] Prof. Dr. C. Lambert
Institut für Organische Chemie
Bayerische Julius-Maximilians-Universität Würzburg
Am Hubland, 97074 Würzburg (Germany)

[c] Dr. J. C. Cherryman, Dr. D. R. Tackley, Dr. S. Leeming, Dr. B. Brown
Avecia Ltd.
PO Box 42, Hexagon House
Blackley, Manchester, M9 8ZS (UK)

Supporting information for this article is available on the WWW under http://www.chemeurj.org/ or from the author.

 **DOI: 10.1002/chem.200305200**  

biphenyl)-4,4′-diamine (TPD, **1a**), a classic polyarylamine based hole transport material.[4a] This work concluded that, at least in an idealised gas environment, oxidation would be accompanied by planarisation and adoption of partial quinoidal character in the biphenyl group, with rotation of the peripheral aryl groups about the N–$C_{aryl}$ bond to positions approximately orthogonal to the biphenyl plane. Given the relatively low energy of aryl ring rotation about a single bond, it was suggested that the reorganisation energy term associated with the hole transport process should be dominated by structural changes associated with the biphenyl moiety.[4] However, experimental evidence for these structural changes is scarce. We now report the solid state structures of both *N*,*N*′-diphenyl-*N*,*N*′-bis(2,4-dimethylphenyl)-(1,1′-biphenyl)-4,4′-diamine (**1b**) and the radical cation derived from this material by chemical oxidation, [**1b**]$SbCl_6$. This latter compound is the first crystallographically characterised example of an oxidised hole-transport material. In addition to the solid state structure, we also provide an analysis of the electronic spectra of these materials, including the NIR, or IVCT, absorption band in the radical cations, which provides insight into the role of the peripheral groups on the electronic structure of these radical cations.

## Results and Discussion

Compounds **1a** and **1b** were prepared via standard Ullmann coupling protocols. Closely related procedures have been described previously.[7] Compound **1b** differs from **1a** by virtue of the methyl group *ortho* and *para* to the amine centres on two of the four peripheral ring systems The *ortho* groups were expected to have some impact on the overall geometry of the compound in both the neutral and oxidised forms, particularly with respect to the orientation adopted by the peripheral phenyl rings, and were introduced to improve the solubility and crystallinity of the product.

Cyclic voltammetry (CV) studies of **1a** and **1b** revealed two, reversible one electron waves associated with the formation of the cation radicals [**1a**]$^{+\bullet}$, [**1b**]$^{+\bullet}$ and dications [**1a**]$^{2+}$, [**1b**]$^{2+}$ (Table 1). The first oxidation of the *bis*-methylated compound **1b** was thermodynamically more favourable than in the case of **1a**, possibly due to the inductive effect of the methyl groups in the *ortho* and *para* positions. The second oxidation potentials were essentially the same. The potential difference between these two redox processes allows an estimate of the thermodynamic stability of the radical cation, **1**$^{+\bullet}$, with respect to disproportionation to **1** and **1**$^{2+}$ at ambient temperature (**1a** $K_c$=4300, **1b** $K_c$=20500).[8] For similar systems, $K_c$ values of similar magnitude are common;[2b] this suggests that the radical cations may be suitable targets for preparative studies.

In order to assess the kinetic stability of these compounds, and to follow the oxidation event in situ, room temperature UV/Vis-NIR spectroelectrochemical studies were undertaken. The observation of sharp isosbestic points during the electrolytic cycle **1**→**1**$^{+\bullet}$→**1**$^{2+}$→**1**$^{+\bullet}$→**1**, and recovery of the original spectra of **1** at the end of the cycle confirm both the chemically reversible nature of the redox system in $CH_2Cl_2$ and the chemically distinct nature of each member of the redox series (Figure 1).

For each compound, a set of π–π* bands are observed in the electronic spectrum, which shift to lower energy upon the oxidation from the neutral material (**1a** 310, 353 nm, **1b** 305, 350 nm), through the radical cations (**1a**$^{+\bullet}$ 484; **1b**$^{+\bullet}$ 476 nm) to the dications (**1a**$^{2+}$ 730; **1b**$^{2+}$ 749 nm). The radical cations **1**$^{+\bullet}$ also display unique bands in the NIR region (**1a** 1400; **1b** 1347 nm). These electronic transitions are analysed in more detail below. At this point we simply wish to note that the π–π* transitions in the dicationic species are essentially identical in energy and band shape to those observed for oxidised triaryl (mono)amines [$NAr_3$]$^{+\bullet}$;[9] this indicates that **1**$^{2+}$ can be described approximately in terms of two localised triaryl cations. However, **1**$^{2+}$ is ESR silent at room temperature, presumably due to strong antiferromagnetic coupling.

Chemical oxidation of **1a** with one equivalent of $SbCl_5$ in $CH_2Cl_2$ resulted in the immediate formation of a dark orange solution of the radical cation, although we have not yet succeeded in isolating crystalline material from this solution. Oxidation of **1b** produced a similarly coloured solution, from which dichroic, needle-like crystals of [**1b**]$SbCl_6$ with a metallic lustre were obtained, following addition of hexane. The electronic spectrum of material isolated in this way was essentially identical to that observed spectroelectrochemically for the radical cation, with only minor deviations in band shape and energy of the NIR band arising from ion-pairing effects with the supporting electrolyte.

To the best of our knowledge, there is only a single report describing the solid state structures of *N*,*N*,*N*′,*N*′-tetraaryl-

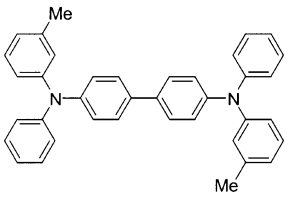


**1a**

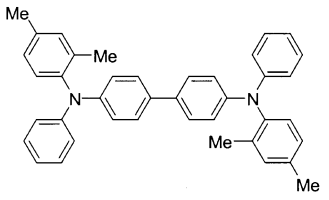


**1b**

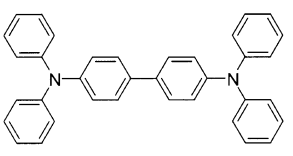


**1c**

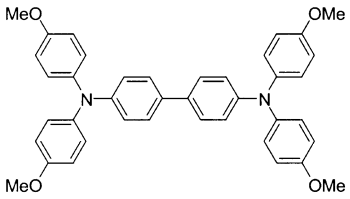


**2**

Table 1. Half-wave Potential ($E_{1/2}$ vs $Fc/Fc^+$) and difference between first and second redox process ($\Delta E$) for **1a**, **1b** and **2**.

| | **1a**[a] | **1b**[a] | **2**[b] |
|---|---|---|---|
| $E_{1/2}$ [V] | 0.292 | 0.250 | 0.085 |
| $E_{1/2}$ [V][a] | 0.507 | 0.505 | 0.305 |
| $\Delta E$ [V] | 0.215 | 0.255 | 0.220 |
| $K_c$ | 4300 | 20500 | 5250 |

[a] 0.1 M $NBu_4BF_4/CH_2Cl_2$ at 100 mV $s^{-1}$. [b] 0.1 M $NBu_4PF_6/CH_2Cl_2$ at 250 mV $s^{-1}$ (from ref. [17a]).



 

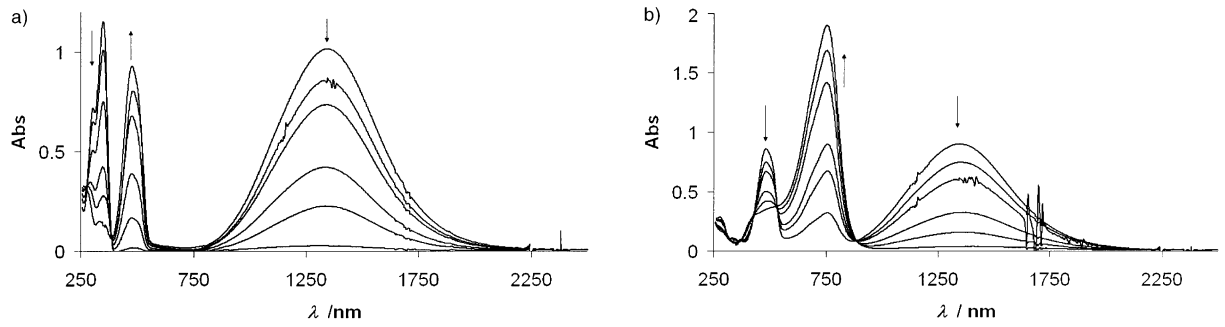


Figure 1. UV/ Vis-NIR spectroelectrochemistry of **1b** during sequential oxidation to $\mathbf{1b}^{+\cdot}$ (left) and $\mathbf{1b}^{2+}$ (right) ($CH_2Cl_2$, 0.1 M $NBu_4BF_4$). The arrows indicate the bands which grow and decay during the electrolysis. $\lambda(cm^{-1})/\varepsilon$ ($mol^{-1}dm^3cm^{-1}$) **1a** 28410/40150; **1b** 27170/35300; $\mathbf{1a}^{+\cdot}$ 7500/37800; $\mathbf{1b}^{+\cdot}$ 7800/30680; $\mathbf{1a}^{2+}$ 13740/74800; $\mathbf{1b}^{2+}$ 13330/56590.

(1,1′-biphenyl)-4,4′-diamine derivatives which were determined using synchrotron based single crystal and powder X-ray diffraction methods, with the single-crystal data complicated by a significant degree of rotational disorder.[10] No solid state structural data from the radical cations derived from such materials have been reported to date. Given the interest in molecular conformation of species such as **1** and $\mathbf{1}^{+\cdot}$ single crystal X-ray diffraction studies of $\mathbf{1b}\cdot CH_2Cl_2$ and $[\mathbf{1b}]SbCl_6\cdot 0.5\,CH_2Cl_2$ were undertaken, using crystals grown from $CH_2Cl_2$/hexane mixtures (Table 2).

For the neutral molecule $\mathbf{1b}\cdot CH_2Cl_2$ (Figure 2, Table 3), a planar conformation is found at the nitrogen centres, with N–C(7,13) bond lengths of 1.417(5) and 1.441(5) Å, the longer N–C distance associated with the 2,4-dimethyl substituted ring. The $N–C4_{(biphenyl)}$ bond length is 1.415(5) Å. The central C1–C1′ bond in the biphenyl moiety is 1.483(7) Å, and the bond lengths within the rings of the biphenyl group range between 1.387(5)–1.410(5) Å. There are no unusual C–C bond lengths within the peripheral phenyl groups. The torsion angles are summarised in Table 3, and define the propeller-like geometry about the nitrogen centres with respect to the plane defined by the three N–C bonds. A two-fold axis passes mid-way between C1 and C1′ and relates the two halves of the molecule. The twist angle between the symmetry related rings of the biphenyl moiety is 37.1(3)° [C2-C1-C1′-C6′]. When compared to the orientation of the unsubstituted ring [C4-N1-C7-C8 –34.3(6)°], the methyl substituted ring [C13–C18] is twisted considerably out of the $NC_3$ plane [C4-N1-C13-C14 –66.0(5)°], no doubt due to the steric effect of the C19 methyl group. The decreased overlap between the aromatic π system and the nitrogen lone pair which results is responsible for the increased N–C13 bond length noted above. With the exception of these steric constraints, the structure is very similar to the optimised geometry of **1a** obtained using DFT methods (Table 3).

The molecular packing of $\mathbf{1b}\cdot CH_2Cl_2$ (Figure 3) shows a layered structure with the layers running perpendicular to the *b* axis. The molecules of each layer are out of register with those in the layer immediately above and below, giving an ABA motif. When viewed along the *b* axis, the molecules form column-like stacks, with the adjacent stacks interdigitated to accommodate the *para* methyl groups. The disordered solvent molecules are found in the channels formed between these columns.

Table 2. Crystal data and structure refinement parameters for $\mathbf{1b}\cdot CH_2Cl_2$ and $[\mathbf{1b}]SbCl_6\cdot 0.5\,CH_2Cl_2$.

| | $\mathbf{1b}\cdot CH_2Cl_2$ | $[\mathbf{1b}]SbCl_6\cdot 0.5\,CH_2Cl_2$ |
|---|---|---|
| formula | $C_{41}H_{38}Cl_2N_2$ | $C_{40.5}H_{37}Cl_7N_2Sb$ |
| $F_w$ | 629.63 | 921.62 |
| $T$ [K] | 100(2) | 120(2) |
| $\lambda$ [Å[ ($Mo_{K\alpha}$) | 0.71073 | 0.71073 |
| dimensions [$mm^3$] | $0.38\times0.10\times0.08$ | $0.46\times0.13\times0.05$ |
| crystal system | monoclinic | orthorhombic |
| space Group | *C*2/*c* | *Pccn* |
| *a* [Å] | 26.379(2) | 23.631(2) |
| *b* [Å] | 9.332(1) | 11.282(1) |
| *c* [Å] | 15.022(1) | 15.767(1) |
| $\beta$ [°] | 111.07(3) | 90 |
| $V$ [$Å^3$] | 3450.7(8) | 4203.7(7) |
| $Z$ | 4 | 4 |
| $\rho_{calcd}$ | 1.212 | 1.456 |
| μ [$mm^{-1}$] | 0.219 | 1.132 |
| $2\theta_{max}$ | 51.98 | 56.56 |
| refls colld (unique) | 14624 (3406) | 24596 (5210) |
| max min$^{-1}$ transmission | 0.983/0.921 | 0.937/0.747 |
| $R$ ($I>2\sigma I_o$)/$wR$ (all data) | 0.0921/0.2726 | 0.0854/0.3037 |

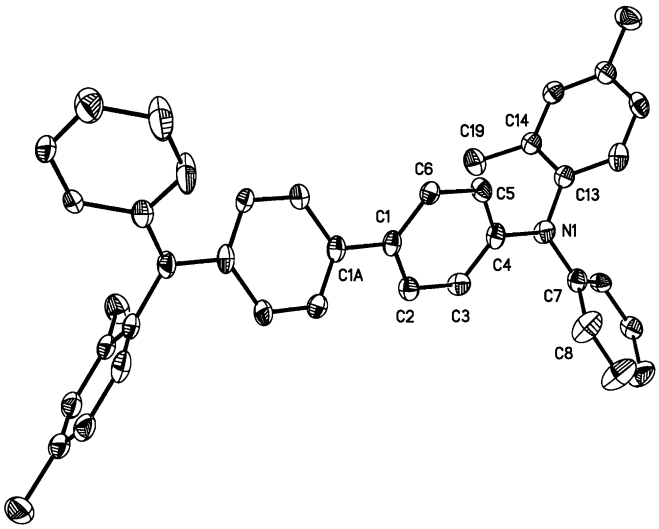


Figure 2. A 50% probability ORTEP plot of **1b** showing the atom labelling scheme. In this and subsequent Figures, H-atoms are omitted for clarity.

  

Table 3. Bond lengths [Å], bond and torsion angles [°] for **1a**, **1a**$^{+\cdot}$, **1b**, **1b**$^{+\cdot}$.

| | **1a**[a] | **1a**$^{+\cdot}$[a] | **1b** | | **1b**$^{+\cdot}$ | |
|---|---|---|---|---|---|---|
| | | | [a] | [b] | [a] | [b] |
| N1–C4 | 1.422 (1.42) | 1.401 (1.39) | 1.419 | 1.415(5) | 1.397 | 1.391(8) |
| N1–C7 | 1.425 (1.42) | 1.431 (1.43) | 1.423 | 1.417(5) | 1.429 | 1.420(8) |
| N1–C13 | 1.426 | 1.432 | 1.436 | 1.441(5) | 1.439 | 1.445(9) |
| C1–C1′ | 1.482 (1.48) | 1.467 (1.46) | 1.480 | 1.483(7) | 1.463 | 1.458(11) |
| C1–C2 | 1.414 (1.41) | 1.422 (1.42) | 1.413 | 1.410(5) | 1.423 | 1.419(9) |
| C2–C3 | 1.396 (1.39) | 1.388 (1.38) | 1.397 | 1.392(5) | 1.388 | 1.386(9) |
| C3–C4 | 1.412 (1.40) | 1.421 (1.42) | 1.412 | 1.396(6) | 1.421 | 1.392(9) |
| C4–C5 | 1.412 | 1.421 | 1.414 | 1.400(5) | 1.423 | 1.409(9) |
| C5–C6 | 1.396 | 1.388 | 1.395 | 1.387(5) | 1.387 | 1.366(8) |
| C4-N1-C7 | 120.1 (120) | 120.8 (120) | 121.5 | 122.2(3) | 121.6 | 122.3(5) |
| C4-N1-C13 | 120.0 (120) | 120.7 (120) | 119.3 | 119.3(3) | 120.4 | 119.5(5) |
| C7-N1-C13 | 119.9 (120) | 118.5 (120) | 118.6 | 118.1(3) | 117.9 | 118.1(5) |
| C2-C1-C1′-C6′ | 34.7 (33.8) | 24.8 (23.0) | 32.1 | 37.1(3) | 24.0 | 4.1(11) |
| C7-N1-C4-C3 | 39.3 (42.0) | 29.8 (25.8) | −40.2 | −37.1(6) | 151.0 | 166.3(7) |
| C13-N1-C4-C3 | 39.6 | 29.9 | 149.0 | 150.4(4) | −24.4 | −16.5(9) |
| C4-N1-C7-C8 | 41.0 (40.6) | 45.3 (47.6) | −30.9 | −34.3(6) | −40.1 | −54.7(10) |
| C13-N1-C7-C8 | 40.6 | 45.2 | 140.0 | 138.3(4) | 135.5 | 128.1(8) |
| C4-N1-C13-C14 | 41.3 (42.3) | 44.4 (49.3) | −63.1 | −66.0(5) | 120.2 | 110.7(8)[c] |
| C7-N1-C13-C14 | 41.7 | 44.5 | 125.8 | 121.2(4) | −55.4 | −71.9(9)[c] |

[a] DFT optimised structural parameters, with data from ref. [4a] in parentheses for comparison. [b] Crystallographically determined parameters. [c] Values from main component of the disordered substituted phenyl ring.

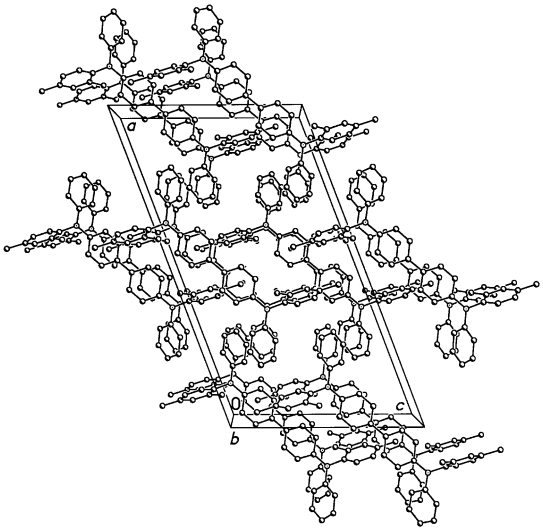


Figure 3. Molecular packing in the crystal of **1b**·0.5 $CH_2Cl_2$ viewed down the *b* axis. The disordered solvent molecules have been omitted for clarity.

The radical cation **1b**$^{+\cdot}$ (Figure 4, Table 3) also displays a planar geometry about the nitrogen centres, and the N–C(7,13) bond lengths to the peripheral aryl ring systems [1.420(8), 1.445(9) Å] are similar to those found in **1b**. The substituted ring is disordered over two sites (66/34 occupancy), which are related by a 180° rotation around the N1–C13 bond. In contrast to the structure of **1b**, the radical cation **1b**$^{+\cdot}$ has $C_i$ symmetry. The biphenyl group has rotated into a position closer to the $NC_3$ plane [C3-C4-N1-C13 −16.5(9)°], and the twist angle between the biphenyl ring systems [C6-C1-C1′-C2′] has decreased to only 4.1(1.1)°. The N–$C4_{(biphenyl)}$ bond length [1.391(4) Å] is significantly shorter than the N–C(7,13) bonds in either structure. However, the C1–C1′ bond length [1.46(1) Å] in **1b**$^{+\cdot}$ is equivalent, within error, to that in **1b**. While not strictly of statistical significance, it is still worth noting that C2–C3 [1.386(9) Å] and C5–C6 [1.366(8) Å] fall at the shorter end of the range of C–C bond lengths in the biphenyl rings [1.366(8)–1.419(9) Å].

Electronic structure calculations indicate that the HOMO in species such as **1b**$^{+\cdot}$ is delocalised over the N-$C_6H_4$-$_6H_4$-N moiety.[12] Consequently, the bond lengths in **1b** and **1b**$^{+\cdot}$ are not expected to be particularly sensitive to the oxidation state of the compound, as the fraction of electronic charge lost upon oxidation will be divided over all the atoms in the benzidene moiety. Nevertheless, the net result of oxidation is a marginal decrease in the N···N separation from 9.981(6) Å in **1b** to 9.89(1) Å in the radical cation **1b**$^{+\cdot}$. When the structure of the radical cation **1b**$^{+\cdot}$ is compared with that of the neutral molecule **1b**, using the C4-C7-C13 plane as a point of reference, the greatest changes to the structure are associated with the relative orientation of the C7–C12 aryl ring and the biphenyl moiety. These geometric changes observed between **1b** and **1b**$^{+\cdot}$ are largely in agreement with those predicted using high-level calculations (Table 3).[4a]

In the crystal structure of [**1b**]$SbCl_6$·0.5 $CH_2Cl_2$, layers of radical cations are found arranged perpendicular to the *a* axis, in a herringbone motif. Between these layers, the $SbCl_6^-$ anions and molecules of $CH_2Cl_2$ are found forming a second layer. The crystal structure can be regarded therefore as alternating layers of opposite charges, which is similar to the structural motifs found in many conducting organic materials (Figure 5). Within the solvent and anion layer, the anions form chains aligned with the *c* axis by symmetry constraints, with an inter-anion Cl···Cl distance of 3.202(5) Å, which is 0.3 Å less than twice the van der Waals radius of Cl. In addition to the electrostatic interactions between the layers of opposite charge, there is a close contact between H3 of the biphenyl moiety and Cl4 of the $SbCl_6^-$ anion (H3···Cl4 2.75 Å, C3-H3-Cl4 145.4°). Each $SbCl_6$ anion resides in a vacancy created by four cations and the location of the anion with respect to the nitrogen centres in any one cation is distinctly asymmetric [N1···Sb 6.974(5) Å, N1′···Sb 9.276(5) Å]. However, within the extended lattice each N centre is found in an identical environment, being located 6.974(5) Å from two anions and 7.446(5) Å from two others.

Formally, the radical cations **1**$^{+\cdot}$ can be considered as organic "mixed-valence" compounds, and the NIR absorption bands present in these species are related to the inter-valence charge transfer (IVCT) band described in Hush theory for moderately coupled (Class II) mixed-valence compounds.[11,12] As the reorganisation energy of the system, $\lambda$, decreases relative to the coupling energy, *V*, the thermal

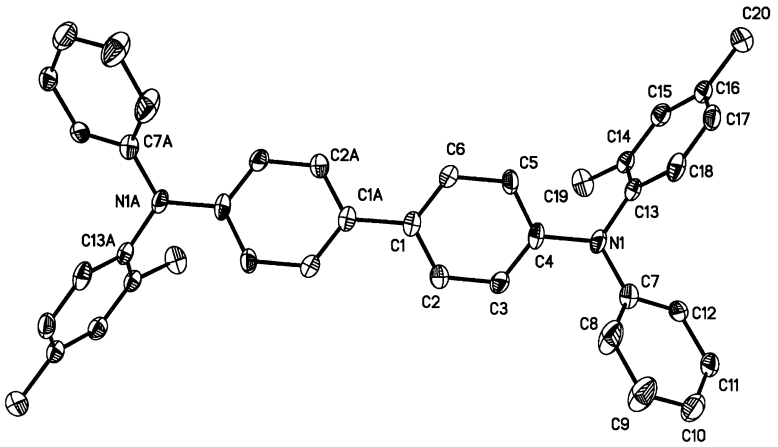


Figure 4. A 50% probability ORTEP plot of the cation $\mathbf{1b}^{+\cdot}$ showing the atom labelling scheme. For the substituted phenyl ring, only the main component of the disordered ring is shown.

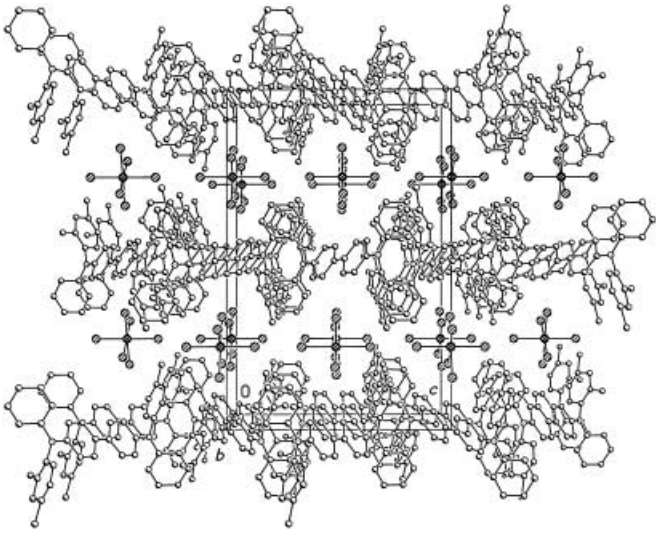

Figure 5. Molecular packing in the crystal of $[\mathbf{1b}]SbCl_6 \cdot CH_2Cl_2$ showing the layered structure viewed down the *b* axis. The disordered solvent has been omitted for clarity.

barrier to *intra*molecular electron transfer, $\Delta G^*$, decreases ($\Delta G^* = \lambda/4 - V + V^2/\lambda$) and becomes zero when $\lambda = 2\ V$.[12] At this point, the system is said to be Class III (delocalised), and the Gaussian-shaped "IVCT" band is "cut-off" at $\lambda = 2$ V. In the delocalised (Class III) systems, where neither intra-molecular charge transfer nor formal oxidation states associated with different sites are appropriate concepts, the use of terms such as "IVCT" are not precise, but in the absence of a more descriptive language, and in keeping with convention, we use this term to describe the NIR transition. There is a great deal of interest at present in the analysis of systems at the borderline between Class II and Class III,[14,15] and we have taken advantage of the availability of samples of $[\mathbf{1b}]SbCl_6$ to record spectra in a range of solvents without the complications of supporting electrolyte inherent in spectroelectrochemically generated data. The spectrum of $\mathbf{1a}^{+\cdot}$ in pure $CH_2Cl_2$ was obtained by titration of a $CH_2Cl_2$ solution of **1a** with a solution of $SbCl_5$ in the same solvent.

While the high energy side of the NIR band in $[\mathbf{1}]SbCl_6$ can be fitted to a single Gaussian function, the band as a whole is distinctly non-Gaussian in shape, as expected for these strongly coupled radicals (Table 4).[14]–[18] In the case of $\mathbf{1b}^{+\cdot}$ the band energy, $\tilde{\nu}_{max}$, and shape was remarkably independent of solvent, only shifting appreciably from the values measured in $CH_2Cl_2$ in strongly polar solvents, such as propionitrile, where the band maximum is about 400 $cm^{-1}$ higher in energy.[19]

The asymmetric band shape, and independence of the band maximum with solvent observed for $\mathbf{1b}^{+\cdot}$, suggests

Table 4. NIR band and derived parameters from of $\mathbf{1a}^{+\cdot}$,[a] $\mathbf{1b}^{+\cdot}$[a] and $\mathbf{2}^{+\cdot}$[b] at 298 K.

| | $\mathbf{1b}^{+\cdot}$ PhBr | $\mathbf{1b}^{+\cdot}$ $CHCl_3$ | $\mathbf{1b}^{+\cdot}$ PhCN | $\mathbf{1b}^{+\cdot}$ EtCN | $\mathbf{1a}^{+\cdot}$ $CH_2Cl_2$ | $\mathbf{1b}^{+\cdot}$ $CH_2Cl_2$ | $\mathbf{2}^{+\cdot}$ $CH_2Cl_2/NBu_4PF_6$ |
|---|---|---|---|---|---|---|---|
| $\tilde{\nu}_{max}$ [$cm^{-1}$] | 7363 | 7363 | 7545 | 7770 | 7120 | 7380 | 6360 |
| $\varepsilon$ [$M^{-1}cm^{-1}$] | 22600 | 30750 | 23160 | 16700 | 37800 | 24600 | 28040 |
| $E_N^T$ | 0.209 | 0.259 | 0.333 | 0.401 | 0.309 | 0.309 | 0.323[c] |
| $\tilde{\nu}_{1/2(high)}$ [$cm^{-1}$][d] | 3574 | 3614 | 3650 | 3360 | 3630 | 3880 | 3750 |
| $\tilde{\nu}_{1/2(low)}$ [$cm^{-1}$][e] | 2526 | 2486 | 2590 | 2490 | 2400 | 2460 | 2590 |
| $\tilde{\nu}_{1/2(obs)}$ [$cm^{-1}$][f] | 3050 | 3050 | 3120 | 2925 | 3015 | 3170 | 3170 |
| $\tilde{\nu}_{1/2(HTL)}$ [$cm^{-1}$][g] | 4113 | 4113 | 4164 | 4225 | 4045 | 4118 | 3820 |
| $\tilde{\nu}_{1/2(high)}/\tilde{\nu}_{1/2(HTL)}$ | 0.87 | 0.87 | 0.87 | 0.79 | 0.89 | 0.94 | 0.98 |
| $\tilde{\nu}_{1/2(high)}/\tilde{\nu}_{1/2(low)}$ | 1.41 | 1.45 | 1.41 | 1.35 | 1.51 | 1.57 | 1.45 |
| $V$ [$cm^{-1}$] | | | | | 3200 | 3300 | 2800[h] |
| $\lambda$ [$cm^{-1}$] | | | | | 7500 | 7800 | 6800[h] |
| $l$ [$cm^{-1}$] | | | | | 3100 | 2700 | 2800[h] |
| $\Delta G^{\neq}$ [$cm^{-1}$] | | | | | 50 | 50 | 60[h] |

[a] As $SbCl_6^-$ salt. [b] Spectroelectrochemically generated data from ref. [17a]. [c] Pseudo-$E_N^T$ parameter calculated to allow for the effects of the supporting electrolyte used in the spectroelectrochemical experiment; see ref. [17a]. [d] Twice the bandwidth at half-height of the high-energy side. [e] Twice the bandwidth at half-height of the low-energy side. [f] Observed halfwidth at half-height. [g] Calculated from $\tilde{\nu}_{1/2(HTL)} = 47.94[\tilde{\nu}_{max}]^{1/2}$. [h] These values were obtained by the same fit procedure as described in the text for $\mathbf{1b}^{+}$.

  

that, at least in a relatively non-polar media, these cations are approaching fully delocalised (Class III) structures. As such, the electronic coupling parameter $V$ for $\mathbf{1a}^{+\cdot}/\mathbf{1b}^{+\cdot}$ can be estimated to be 3560/3680 $cm^{-1}$ in $CH_2Cl_2$ [Eq. (2)].

$$V = \tilde{\nu}_{max}/2 \quad (2)$$

Alternatively, semi-classical Marcus–Hush theory for the degenerate case may be used to extract the relevant parameters from the spectroscopic data. In order to perform this analysis, a vibronic matrix [Eq. (3)] with one asymmetric mode $x$ (the ET coordinate) and one totally symmetric mode $y$, similar to the one given by Piepho[20] and Schatz,[21] was constructed.

$$\begin{vmatrix} V + l_x x + \lambda_x x^2 + l_y y + \lambda_y y^2 - \varepsilon & V + l_y y \\ V + l_y y & V - l_x x + \lambda_x x^2 + l_y y + \lambda_y y^2 - \varepsilon \end{vmatrix} = 0$$

The vibronic matrix is presented here in the context of a localised electronic basis, where the basis functions represent diabatic (non-interacting) states in which the hole (or unpaired electron) is localised at one of the two redox centres. The diabatic potentials are expanded as power series which are terminated after the quadratic terms for the diagonal elements and after the linear terms for the off-diagonal elements. In this matrix, $V$ is the electronic coupling parameter, $\lambda_x$ and $\lambda_y$ are the reorganisation energies for the $x$ and $y$ mode, respectively, $l_x$ and $l_y$ are the linear vibronic coupling constants. The (dimensionless) displacement of the upper adiabatic surface and the ground state surface along the y mode is given by $\delta Q_y = l_y/\lambda_y$ and along the $x$ mode it is $\delta Q_x = l_x/2\lambda_x$. Thus, choosing $l_x = \lambda_x$ places the minima of the diabatic potentials at $x = \pm 0.5$. Furthermore, we make the simplification that $\lambda_x = \lambda_y = \lambda$. Diagonalisation of the matrix gives two adiabatic potential energy surfaces. Using a Boltzmann distribution of infinitesimally spaced vibrational states and the energy difference between the two adiabatic potential energy surfaces, we calculated the absorption spectra.[22] As long as the coupling $V$ is rather strong, the spectra can be fitted accurately by adjusting $V$, $l_y$ and $\lambda$. Thus, in contrast to the traditional one-dimensional Marcus–Hush theory, no assumptions about any effective (diabatic) electron transfer distance are necessary. We note that similar spectral simulations using this vibronic matrix but with the full dynamic solutions in the diabatic approximation have been reported by Coropceanu et al. for $\mathbf{2}^{+\cdot}$.[18a]

Fitting the experimental spectra of $\mathbf{1a}^{+\cdot}$ and $\mathbf{1b}^{+\cdot}$ (see for example, Figure 6) in the manner described by Equation (2) allows an estimate of not only the electronic coupling parameter $V$ ($\mathbf{1a}^{+\cdot}$ 3200 $cm^{-1}$; $\mathbf{1b}^{+\cdot}$ 3300 $cm^{-1}$), but also the reorganisation energy $\lambda$($\mathbf{1a}^{+\cdot}$ 7500 $cm^{-1}$; $\mathbf{1b}^{+\cdot}$ 7800 $cm^{-1}$), and the linear coupling constant $l$ ($\mathbf{1a}^{+\cdot}$ 3100 $cm^{-1}$; $\mathbf{1b}^{+\cdot}$ 2700 $cm^{-1}$) of the symmetric mode (Table 4). These parameters are similar to those derived from the radical cation derived from *N*,*N*,*N*′,*N*′-tetra-4-methoxyphenyl-4,4′-diamino-1,1′-biphenyl (**2**) (Table 4), which has been shown to fall near the Class II/III borderline and exhibits a modestly solvent dependent IVCT band.[14,15,18a] This band in the NIR region has been shown to contain a significant contribution from redistribution of charge from the peripheral aromatic rings to the benzidene core, and should therefore be expected to be sensitive to the solvent and substituent groups.[18a] In the case of $\mathbf{2}^{+\cdot}$ the internal contribution to the reorganisation energy has been evaluated from plots of the NIR band energy against the Dimroth–Reichardt solvent parameters. Extrapolation of the plot to the gas phase gives $\lambda_v = 3200$ $cm^{-1}$, a value approximately half of the total reorganisation energy $\lambda = \tilde{\nu}_{max}$ in 0.1 M $NBu_4PF_6/CH_2Cl_2$ (6360 $cm^{-1}$). Similar treatment of data from $\mathbf{1b}^{+\cdot}$ gives $\lambda_v = 6830$ $cm^{-1}$, or about 90% of the total reorganisation energy in $CH_2Cl_2$ (Table 4). Clearly, direct comparisons between the results from **1** and **2** are to be made with caution as the influence of the solvent medium, including supporting electrolyte in the case of **2**, on the transition energy and band shape are not entirely clear at present.

The fit of the IVCT bands of $\mathbf{1a}^{+}$, $\mathbf{1b}^{+}$ and $\mathbf{2}^{+}$ also yields the activation barrier $\Delta G^{\neq}$ of the intramolecular ET which is about 50 $cm^{-1}$ for all radical cations. Together with the symmetrical structure of $\mathbf{1b}^{+}$ derived from X-ray crystallography, the optical features and the parameters derived by the IVCT band fit strongly suggest that the benzidine radical cations are on the border between Class II and Class III.

It is useful to consider the electronic transitions in terms of the molecular orbitals involved, which in turn are best displayed graphically. Time dependent DFT methods (TDDFT), as contained within the Guassian 98 package, were employed to model the transitions in each of $\mathbf{1a}^{n+}$, $\mathbf{1b}^{n+}$ and the parent compound $\mathbf{1c}^{n+}$ ($n = 0, 1$), and the results displayed graphically using Molekel, as described in the Experimental Section. Geometry optimisations [BPW91/6-31G(d,p)] for both the neutral and radical cation states were carried out, and the results found to be in excellent agreement with the data determined crystallographically. While the B3LYP6-31G** optimised geometry of **1a** and $\mathbf{1a}^{+\cdot}$ have been reported previously,[14] we include our results for consistency in the comparisons.

Analysis of the electronic transitions using TDDFT methods gave essentially identical results for each compound,

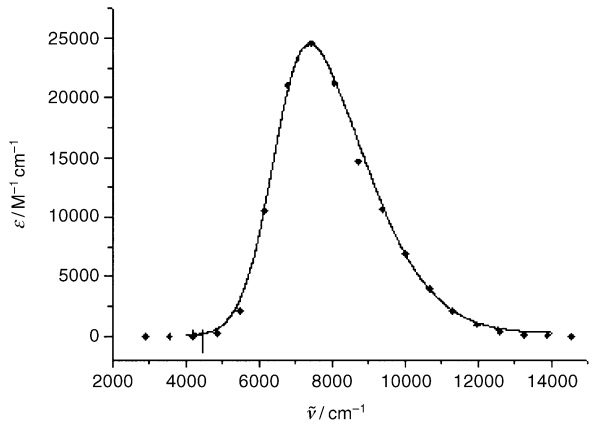


Figure 6. NIR band of [**1b**]$SbCl_6$ (solid line: experiment, diamonds: theoretical fit).

which are summarised in Table 5, and the agreement between calculated transition energies and the experimentally observed results (<0.06 eV) are remarkably good. The critical orbitals involved in the major transitions are illustrated for **1c** (Figure 7) and **1c**$^{+\cdot}$ (Figure 8). Those of **1a,b**$^{n+}$ are similar. The lowest energy absorption band in the neutral species arises from the HOMO–LUMO transition. The HOMO contains appreciable character from the amine nitrogen centres, the biphenyl moiety and the *ortho* and *para* carbons of the peripheral ring systems. The LUMO is heavily centred on the biphenyl group, and may be described approximately as the biphenyl π* system. The higher energy UV transition comprises two almost degenerate transitions arising from HOMO–(LUMO+2) and HOMO–(LUMO+3). These higher lying unoccupied orbitals display extensive aromatic π* character localised on the peripheral ring systems. The two transitions in the UV spectrum of the neutral tetraarylbenzidene moiety can therefore be described satisfactorily in terms of $\pi$–$\pi^*_{\text{biphenyl}}$ and $\pi$–$\pi^*_{\text{peripheral}}$ transitions.

Upon oxidation, these π–π* bands are replaced by a new transition in the visible region. Not surprisingly, analysis of the TDDFT results indicates this transition to be the SOMO–LUMO (α-spin) transition while the NIR absorption band corresponds to the (HOMO−1)–SOMO (β-spin) transition, in keeping with conventional ideas. The graphical representation of these orbitals (Figure 8) clearly shows the (HOMO−1) and SOMO to be delocalised over the molecular framework which supports strongly the conclusions drawn from the band shape analysis described above. We note again for emphasis the confusion which may arise from the description of this transition as an IVCT band.

Table 5. Calculated (TDDFT) and observed electronic transitions.

| | $\lambda_{max}$ | | | |
|---|---|---|---|---|
| | Observed | | Calculated | |
| | [nm] | [eV] | [nm] | [eV] |
| **1a** | 310, 353 | 3.9995, 3.5123 | 305, 306, 358 | 4.0588, 4.0508, 3.4604 |
| **1a**$^{+\cdot}$ | 484, 1400 | 2.5616, 0.8856 | 426, 1423 | 2.9105, 0.8709 |
| **1b** | 305, 350 | 4.0651, 3.5424 | 304, 353 | 4.0792, 3.5041 |
| **1b**$^{+\cdot}$ | 476, 1347 | 2.6047, 0.9205 | 422, 1359 | 2.9347, 0.9120 |
| **1c** | | | 304, 357 | 4.0719, 3.4682 |
| **1c**$^{+\cdot}$ | | | 424, 1417 | 2.9210, 0.8744 |

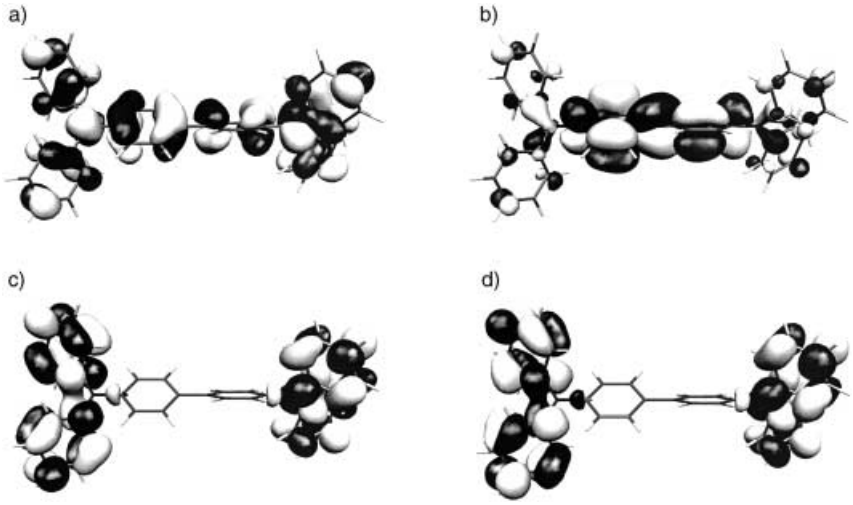


Figure 7. Graphical representation of the HOMO (a), LUMO (b), (LUMO+2) (c) and (LUMO+3) (d) of **1c**.

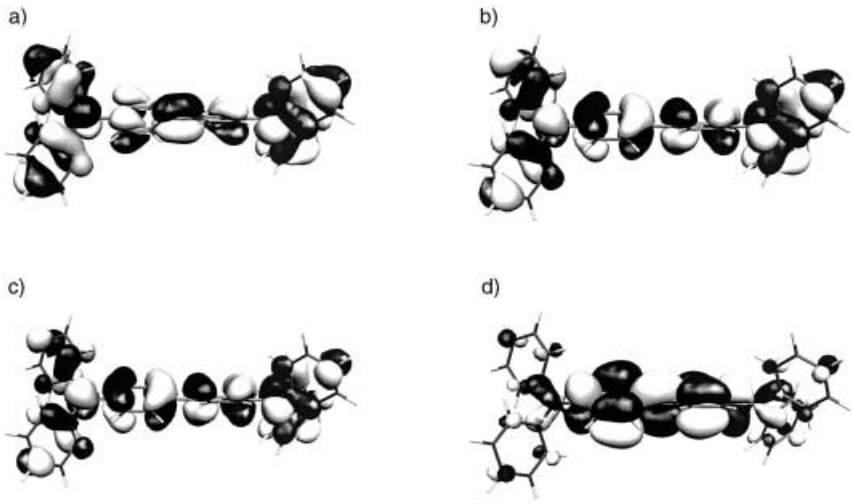


Figure 8. Graphical representation of the (HOMO−1) (*β*) (a), SOMO (*α*, occupied)) (b), SOMO (*β*, virtual) (c), LUMO (*α*, virtual) (d) orbitals of **1c**$^{+\cdot}$.

## Conclusion

The crystallographically determined structures of **1b** and [**1b**]$SbCl_6$ display changes in geometry which confirm the predictions made from DFT calculations. The introduction

  

of pendant groups on the peripheral aryl rings plays some role in determining the static solid state geometry, but the single *ortho* methyl group used in this study does not significantly influence the overall reorganisation energy associated with intramolecular charge transfer, as evidenced by the similar profile of the IVCT band in the compounds $\mathbf{1a}^{+\cdot}$, $\mathbf{1b}^{+\cdot}$ and $\mathbf{2}^{+\cdot}$. All three systems are borderline Class II/III radical cations. However, the greatly reduced solvatochromic nature of the IVCT band in $\mathbf{1b}^{+\cdot}$ when compared with $\mathbf{2}^{+\cdot}$ suggests that solvent interactions with the peripheral ring systems, and consequently the substituents on them, do play a role in the "IVCT" process. This is consistent with the structure of the orbitals involved in the low energy (NIR) transition which feature appreciable character derived from the *para* and *ortho* carbons of the peripheral ring systems.

## Experimental Section

Compounds **1a** and **1b** were prepared by minor modifications of literature procedures, and the spectroscopic data are in good agreement.[7b] Recrystallisation of **1b** by slow diffusion of methanol into a concentration $CH_2Cl_2$ solution afforded small transparent block shaped crystals suitable for single crystal X-ray diffraction.

Treatment of a solution of **1b** (101 mg, 0.18 mmol) in $CH_2Cl_2$ (5 mL) with a solution of $SbCl_5$ (150 mg, 0.18 mmol) in $CH_2Cl_2$ (150 mL) resulted in the immediate formation of a dark orange solution. The solvent was removed in vacuo and the dark brown residue obtained re-dissolved in a minimum volume of $CH_2Cl_2$, and filtered. The filtrate was treated with hexanes (10 mL), and allowed to slowly evaporate to give red-green needle-like crystals of $[\mathbf{1b}]SbCl_6 \cdot 0.5\,CH_2Cl_2$ with a metallic lustre which were suitable for X-ray diffraction. ES(+)-MS: *m/z*: 544 $[M-SbCl_6]^+$]; ES(−)-MS: *m/z*: 335 $[SbCl_6]^-$, 263 $[SbCl_4]^-$.

Cyclic voltammetry was carried out on solutions in $CH_2Cl_2$ containing 0.1 M $NBu_4BF_4$ as supporting electrolyte, and values obtained referenced against an internal ferrocene standard (0.46 V vs SCE). Each wave satisfied the established criteria for electrochemical reversibility. Spectroelectrochemical studies were carried out in an OTTLE cell (1 mm pathlength) of standard design,[23] using a 0.5 mM solution of **1** in $CH_2Cl_2$ containing 0.1 M $NBu_4BF_4$ supporting electrolyte.

**X-ray Crystallography**: Crystallographic data for $\mathbf{1b} \cdot CH_2Cl_2$ and $[\mathbf{1b}]SbCl_6 \cdot 0.5\,CH_2Cl_2$ are listed in Table 2. The data were collected on a Bruker SMART 1 K diffractometer equipped with a CCD-type area detector and an Oxford Cryosystems open flow Nitrogen gas cooling device.[24] Series of narrow $\omega$-scans (0.3°) were performed at several $\phi$-settings in such a way as to cover a sphere of data to a maximum resolution of 0.81 Å (0.75 Å). Cell parameters were determined and refined using the SMART software[25] from the centroid values of 928 (653) reflections with $2\theta$ values between 4.4° (20.6°) and 50.6° (37°). Raw frame data were integrated using the SAINT program[26]. The reflection intensities were corrected for absorption effects by the multi-scan method based on multiple scans of identical and Laue equivalent reflections[27] (min/max transmission factors = 0.921/0.983) and by numerical integration based on measurements and indexing of the crystal faces[28] (min/max transmission factors = 0.747/0.937), respectively. The structures were solved using Direct Methods and refined by full-matrix least squares on $F^2$ using SHELXTL.[28]

All non-hydrogen atoms in $[\mathbf{1b}]$, and all in $[\mathbf{1b}]SbCl_6$ except the ones in the substituted phenyl ring, were refined with anisotropic atomic displacement parameters (adps). Hydrogen atoms were placed geometrically and allowed to ride on their parent C atom with $U_{iso}(H) = 1.2\,U_{eq}(C)$ (1.5 for methyl hydrogens). Idealized C–H distances were fixed at 0.95 Å (0.98 Å for methyl hydrogens). Disordered dichloromethane is also present in both structures. In the first case a whole molecule of DCM is disordered over 4 positions (related by symmetry in pairs) and it was modelled with fixed occupancies of 25% each. The C and Cl atoms were refined with isotropic adps, while the H atoms were neither found nor geometrically placed. In the second case, half a molecule of $CH_2Cl_2$ is disordered over two positions (related by symmetry), modelled with fixed occupancies of 25% each. Again the C and Cl atoms were refined with isotropic adps, but this time the H atoms were geometrically placed (C–H 0.96 Å) and their positions fixed before the final least-squares refinement cycles.

CCDC-209320 and -209321 contain the supplementary crystallographic data for this paper. These data can be obtained free of charge via www.ccdc.cam.ac.uk/conts/retrieving.html, or from the Cambridge Crystallographic Data Centre, 12 Union Road, Cambridge CB2 1EZ, UK; fax: (+44)1223–336033; or email: deposit@ccdc.cam.ac.uk.

**Computational work**: All calculations were run using the Gaussian 98 program.[29] For each molecule, the geometry was optimised for both the neutral and radical cation states at a DFT level using the BPW91 functional (Becke's 1988 exchange functional,[30] with Perdew and Wang's 1991 gradient-corrected correlation functional[31]) in conjunction with the 6-31G(d,p) basis set.[32] Where possible, molecular symmetry constraints were used to simplify the calculations and to aid the interpretation of the results. Using the optimised geometries, Time-Dependent Density Functional Theory (TDDFT) based calculations were solved for excited states. For these calculations, the PBE1PBE functional was used in conjunction with the 6-31G(d) basis set.[33] The TDDFT calculation was solved for 10 excited states in the case of the neutral species and 20 excited states in the case of the radical cation species. In both cases, the calculation was only solved for singlet excitations. Post-processing for visualisation of the molecular orbitals generated by the TDDFT calculation was performed using the Molekel programme.[34]

## Acknowledgememts

This work was supported by the EPSRC and Avecia Ltd. Professor Howard holds an EPSRC Senior Research Fellowship. The work in Würzburg was supported by the Deutsche Forschungsgemeinschaft (Graduiertenkolleg "Elektronendichte") and the Fonds der Chemischen Industrie. We gratefully acknowledge the assistance of Dr. E. McInnes (EPSRC National ESR Service, University of Manchester), Dr. A. Beeby (Department of Chemistry, University of Durham) and Prof. S. Nelson (Department of Chemistry, University of Wisconsin) for their assistance and helpful discussions.

[1] a) V. Bulvic, G. Gu, P. E. Burrows, S. R. Forrest, M. E. Thompson, *Nature* **1996**, *380*, 29–29; b) N. Tamoto, C. Adachi, K. Nagai, *Chem. Mater.* **1997**, *9*, 1077–1085; c) E. Bellmann, S. E. Shaheen, S. Thayumanavan, S. Barlow, R. H. Grubbs, S. R. Marder, B. Kippelen, N. Peyghambarian, *Chem. Mater.* **1998**, *10*, 1668–1676; d) M. C. Harris, S. L. Buchwald, *J. Org. Chem.* **2000**, *65*, 5327–5333; e) U. Mitschke, P. Bäuerle, *J. Mater. Chem.* **2000**, *10*, 1471–1507; f) P. M. Borsenberger, D. S. Weiss, *Organic Photoreceptors for Xerography*, Marcel Dekker, New York, **1998**.

[2] a) J. Cornil, N. E. Gruhn, D. A. dos Santos, M. Malagoli, P. A. Lee, S. Barlow, S. Thayumanavan, S. R. Marder, N. R. Armstrong, J. L. Brédas, *J. Phys. Chem. A* **2001**, *105*, 5206–5211; b) E. Bellmann, S. E. Shaheen, R. H. Grubbs, S. R. Marder, B. Kippelen, N. Peyghambarian, *Chem. Mater.* **1999**, *11*, 399–407.

[3] a) J. Cornil, D. Beljonne, J.-P. Calbert, J. L. Brédas, *Adv. Mater.* **2001**, *13*, 1053–1067; b) M. Malogoli, M. Manoharan, B. Kippelen, J. L. Brédas, *Chem. Phys. Lett.* **2002**, *354*, 283–290.

[4] a) M. Malagoli, J. L. Brédas, *Chem. Phys. Lett.* **2000**, *327*, 13–17; b) K. Sakanoue, M. Matoda, M. Sugimoto, S. Sakaki, *J. Phys. Chem. A* **1999**, *103*, 5551–5556; c) N. E. Gruhn, D. A. da Silva Filho, T. G. Bill, M. Malagoli, V. Coropceanu, A. Khan, J. L. Brédas, *J. Am. Chem. Soc.* **2002**, *124*, 7918–7919; d) K. Sakanoue, M. Motoda, M. Sugimoto, S. Sakaki, *Nonlinear Opt.* **2000**, *26*, 271–278.

[5] C. Adachi, K. Nagai, N. Tamoto, *Appl. Phys. Lett.* **1995**, *66*, 2679–2681.

[6] See C. Lambert, G. Nöll, J. Schelter, *Nat. Mater.* **2002**, *1*, 69–73, and references therein.
[7] For procedures to similar compounds, see a) S. Thayumanavan, S. Barlow, S. R. Marder, *Chem. Mater.* **1997**, *9*, 3231–3235; b) M. J. Plater, T. Jackson, *J. Chem. Soc. Perkin Trans. 1* **2001**, 2548–2552.
[8] D. E. Richardson, H. Taube, *Inorg. Chem.* **1981**, *20*, 1278–1285.
[9] F. A. Neugebauer, S. Bamberger, W. R. Groh, *Chem. Ber.* **1975**, *108*, 2406–2415.
[10] A. R. Kennedy, W. E. Smith, D. R. Tackley, W. I. F. David, K. Shankland, B. Brown, S. J. Teat, *J. Mater. Chem.* **2002**, *12*, 168–172.
[11] M. B. Robin, P. Day, *Adv. Inorg. Chem. Radiochem.* **1967**, *10*, 247–422.
[12] a) C. Cruetz, *Prog. Inorg. Chem.*, **1980**, *30*, 1–73; b) B. S. Brunschwig, C. Creutz, N. Sutin, *Chem. Soc. Rev.* **2002**, *31*, 168–184; c) J.-P. Launay, *Chem. Soc. Rev.* **2001**, *30*, 386–397.
[13] a) T. Ito, T. Hamaguchi, H. Nagino, T. Yamaguchi, J. Washington, C. Kubiak, *Science* **1997**, *277*, 660–663; b) K. D. Demadis, C. M. Hartshorn, T. J. Meyer *Chem. Rev.* **2001**, *101*, 2655–2685.
[14] a) S. F. Nelsen, *Chem. Eur. J.* **2000**, *6*, 581–588; b) S. F. Nelson, personal communication.
[15] a) C. Lambert, G. Nöll, *J. Am. Chem. Soc.* **1999**, *121*, 8434–8442; b) V. Coropceanu, C. Lambert, G. Nöll, J. L. Brédas, *Chem. Phys. Lett.* **2003**, *373*, 153–160.
[16] a) S. F. Nelson, J. R. Pladziewicz, *Acc. Chem. Res.* **2002**, *35*, 247–254; b) S. F. Nelson, R. F. Ismagilov, K. E. Gentile, D. R. Powell, *J. Am. Chem. Soc.* **1999**, *121*, 7108–7144; c) S. F. Nelson, R. F. Ismagilov, D. R. Powell, *J. Am. Chem. Soc.* **1997**, *119*, 10213–10222; d) S. F. Nelson, H. Q. Tran, M. A. Nagy, *J. Am. Chem. Soc.* **1998**, *120*, 298–304.
[17] a) C. Lambert, G. Nöll, *Angew. Chem.* **1998**, *110*, 2239–2242, *Angew. Chem. Int. Ed.* **1998**, *37*, 2107–2110; b) C. Lambert, G. Nöll, *Chem. Eur. J.* **2002**, *8*, 3467–3477.
[18] a) V. Coropceanu, M. Malagoli, J. M. André, J. L. Brédas, *J. Am. Chem. Soc.* **2002**, *124*, 10519–10530; b) V. Coropceanu, M. Malagoli, J. M. André, J. L. Brédas, *J. Chem. Phys.* **2001**, *115*, 10409–10416.
[19] Solvent dependence of the electronic transitions associated with Class III compounds has been observed, and it has been suggested that Hush's equations should be modified to account for the refractive index of the solvent. For elegant discussions of this point see S. F. Nelson, H. Q. Tran, *J. Phys. Chem. A* **1999**, *103*, 8139–8144, and references therein.
[20] S. B. Piepho, *J. Am. Chem. Soc.* **1988**, *110*, 6319–6326.
[21] P. N. Schatz *in Mixed Valency Systems: Applications in Chemist, Physics and Biology* (Ed.: K. Prassides), Kluwer, Dordrecht, **1991**, pp. 7–28.
[22] K. Y. Wong, P. N. Schatz, *Prog. Inorg. Chem.* **1981**, *28*, 369–449.
[23] C. M. Duff, G. A. Heath, *Inorg. Chem.* **1991**, *30*, 2528–2535.
[24] J. Cosier, A. M. Glazer, *J. Appl. Crystallogr.* **1986**, *19*, 105–107.
[25] Bruker, SMART-NT, Data Collection Software. Version 5.0. Bruker Analytical X-ray Instruments Inc., Madison, Wisconsin (USA), **1998**.
[26] Bruker, SAINT-NT, Data Reduction Software. Version 5.0. Bruker Analytical X-ray Instruments Inc., Madison, Wisconsin (USA), **1998**.
[27] G. M. Sheldrick, SADABS V2.03, Empirical Absorption Correction Program. University of Göttingen (Germany), **2001**.
[28] Bruker, SHELXTL, Version 5.1, Bruker Analytical X-ray Instruments Inc., Madison, Wisconsin (USA), **1998**.
[29] Gaussian 98, Revision A.11, M. J. Frisch, G. W. Trucks, H. B. Schlegel, G. E. Scuseria, M. A. Robb, J. R. Cheeseman, V. G. Zakrzewski, J. A. Montgomery, Jr., R. E. Stratmann, J. C. Burant, S. Dapprich, J. M. Millam, A. D. Daniels, K. N. Kudin, M. C. Strain, O. Farkas, J. Tomasi, V. Barone, M. Cossi, R. Cammi, B. Mennucci, C. Pomelli, C. Adamo, S. Clifford, J. Ochterski, G. A. Petersson, P. Y. Ayala, Q. Cui, K. Morokuma, P. Salvador, J. J. Dannenberg, D. K. Malick, A. D. Rabuck, K. Raghavachari, J. B. Foresman, J. Cioslowski, J. V. Ortiz, A. G. Baboul, B. B. Stefanov, G. Liu, A. Liashenko, P. Piskorz, I. Komaromi, R. Gomperts, R. L. Martin, D. J. Fox, T. Keith, M. A. Al-Laham, C. Y. Peng, A. Nanayakkara, M. Challacombe, P. M. W. Gill, B. Johnson, W. Chen, M. W. Wong, J. L. Andres, C. Gonzalez, M. Head-Gordon, E. S. Replogle, J. A. Pople, Gaussian, Inc., Pittsburgh PA, **2001**.
[30] A. D. Becke, *Phys. Rev. A* **1988**, *38*, 3098–3100.
[31] J. P. Perdew, K. Burke, Y. Wang, *Phys. Rev. B* **1996**, *54*, 16533–16539; Erratum: J. P. Perdew, K. Burke, Y. Wang, *Phys. Rev. B* **1998**, *57*, 14999.
[32] a) R. Ditchfield, W. J. Hehre, J. A. Pople, *J. Chem. Phys.* **1971**, *54*, 724–728; b) W. J. Hehre, R. Ditchfield, J. A. Pople, *J. Chem. Phys.* **1972**, *56*, 2257–2261; c) P. C. Hariharan, J. A. Pople, *Mol. Phys.* **1974**, *27*, 209–214; d) M. S. Gordon, *Chem. Phys. Lett.* **1980**, *76*, 163–168; e) P. C. Hariharan, J. A. Pople, *Theor. Chim. Acta* **1973**, *28*, 213–222.
[33] a) J. P. Perdew, K. Burke, M. Ernzerhof, *Phys. Rev. Lett.* **1996**, *77*, 3865–3868; erratum: J. P. Perdew, K. Burke, M. Ernzerhof, *Phys. Rev. Lett.* **1997**, *78*, 1386; b) C. Adamo, V. Barone, *J. Chem. Phys.* **1999**, *110*, 6158–6170; c) M. Ernzerhof, G. E. Scuseria, *J. Chem. Phys.* **1999**, *110*, 5029–5036.
[34] S. Portmann, H. P. Lüthi, *Chimia* **2000**, *54*, 766–770.

Received: June 3, 2003 [F5200]

  